

## Accepted Manuscript

### Impaired Endothelial Autophagy Promotes Liver Fibrosis By Aggravating The Oxidative Stress Response During Acute Liver Injury

Maria Ruat, Laia Chavarria, Genís Campreciós, Nuria Suárez-Herrera, Carla Montironi, S. Guixé-Muntet, Jaume Bosch, Scott L. Friedman, Juan Carlos Garcia-Pagán, Virginia Hernández-Gea

PII: S0168-8278(18)32498-X  
DOI: <https://doi.org/10.1016/j.jhep.2018.10.015>  
Reference: JHEPAT 7126

To appear in: *Journal of Hepatology*

Received Date: 23 April 2018  
Revised Date: 30 September 2018  
Accepted Date: 3 October 2018

Please cite this article as: Ruat, M., Chavarria, L., Campreciós, G., Suárez-Herrera, N., Montironi, C., Guixé-Muntet, S., Bosch, J., Friedman, S.L., Garcia-Pagán, J.C., Hernández-Gea, V., Impaired Endothelial Autophagy Promotes Liver Fibrosis By Aggravating The Oxidative Stress Response During Acute Liver Injury, *Journal of Hepatology* (2018), doi: <https://doi.org/10.1016/j.jhep.2018.10.015>

This is a PDF file of an unedited manuscript that has been accepted for publication. As a service to our customers we are providing this early version of the manuscript. The manuscript will undergo copyediting, typesetting, and review of the resulting proof before it is published in its final form. Please note that during the production process errors may be discovered which could affect the content, and all legal disclaimers that apply to the journal pertain.



**Title:**

Impaired Endothelial Autophagy Promotes Liver Fibrosis By Aggravating The Oxidative Stress Response During Acute Liver Injury.

**Author Names:**

Maria Ruat\*<sup>1</sup>, Laia Chavarria\*<sup>1</sup>, Genís Campreciós<sup>1,2</sup>, Nuria Suárez-Herrera<sup>1</sup>, Carla Montironi<sup>3</sup>, Guixé-Muntet S<sup>4</sup>, Jaume Bosch<sup>1,2,4</sup>, Scott L. Friedman<sup>5</sup>, Juan Carlos García-Pagán<sup>1,2</sup> and Virginia Hernández-Gea<sup>1,2</sup>.

1. Barcelona Hepatic Hemodynamic Laboratory, Liver Unit, Hospital Clínic-Institut d'Investigacions Biomèdiques August Pi i Sunyer. University of Barcelona.
2. Centro de Investigación Biomédica Red de enfermedades hepáticas y digestivas
3. Pathology Department, Liver Cancer Translational Research Laboratory, BCLC Group, IDIBAPS, Liver Unit, Hospital Clínic
4. Swiss Liver Centre, Inselspital, Bern University, CH
5. Division of Liver Diseases, Department of Medicine, Icahn School of Medicine at Mount Sinai, New York, U.S.

\*Both authors contribute equally to this work

**Corresponding author:** Virginia Hernández-Gea M.D, Ph.D.

Barcelona Hepatic Hemodynamic Laboratory, Liver Unit, Hospital Clínic, Villarroel 170, Barcelona 08036, Spain. Telephone number: +34932275400 (2209), Fax number: +34 932279856; E-mail address:

**Keywords:** Autophagy, endothelial dysfunction, liver fibrosis, oxidative stress, LSEC, Nrf2, endothelial cell, Atg7, nitric oxide, eNOS

**Electronic word count: 7425**

**Number of figures and tables: 7 figures**

**Conflict of interest:** The authors who have taken part in this study declared that they do not have anything to disclose regarding funding or conflict of interest with respect to this manuscript.

**Financial support:** This work was sponsored by the Instituto de Salud Carlos III (ISCIII) PI14/00182, PI17/00298 and the European Union (Fondos FEDER, "Una

manera de hacer Europa”). CIBERehd is funded by Instituto de Salud Carlos III. MR has a FPI grant from Ministerio de Economía y Competitividad related to SAF2013-44723-R & SAF2016-75767-R. LC has a Juan de la Cierva grant from the Instituto de Salud Carlos III

**Authors' contributions:** M.R. & L.C. designed the research, conceived ideas, performed experiments, and wrote the manuscript. G.C. and N.S-H. performed experiments and analyzed data. C.M. performed the histological analysis. S.G-M, J.B., S.L.F. and J.C.G.-P. critically revised the manuscript. V.H-G. designed the research, conceived ideas, wrote the manuscript, obtained funding and directed the study. All authors edited and reviewed the final manuscript.

**ABSTRACT**

**Background & Aims:** Endothelial dysfunction plays an essential role in initiation and progression of liver injury, yet phenotypic regulation of liver endothelial cells remains unknown. Autophagy is an endogenous protective system whose loss could undermine LSEC integrity and phenotype. The aim of our study was to investigate the role of autophagy in the regulation of endothelial dysfunction and the impact of its manipulation during liver injury.

**Methods:** We analyzed primary isolated liver endothelial cells from Atg7<sup>control</sup> and Atg7<sup>endo</sup> mice as well as rats after CCl<sub>4</sub> induced liver injury. Liver tissue and primary isolated stellate cells were used to analyze liver fibrosis. Autophagy flux, microvascular function, NO bioavailability cellular superoxide content and the antioxidant response were evaluated in endothelial cells.

**Results:** Autophagy maintains liver endothelial cells homeostasis and it is rapidly up-regulated during capillarization *in vitro* and *in vivo*. Pharmacological and genetic downregulation of endothelial autophagy increases oxidative stress *in vitro*. During liver injury *in vivo*, the selective loss of endothelial autophagy leads to cellular dysfunction, reduction in intrahepatic NO, impairment to handle oxidative stress and aggravates fibrosis.

**Conclusions:** Autophagy contributes to maintain endothelial phenotype and protects LSEC from oxidative stress during early phases of the disease. Potentiation of autophagy selectively in LSEC during early stages of liver disease may be an attractive approach to modify the course of the disease and prevent fibrosis progression.

**Electronic word count: 224**

**Lay summary**

Liver endothelial cells are the first liver cell type affected after any kind of liver injury. The loss of their unique phenotype during injury contributes to amplify liver damage by orchestrating the response of the liver microenvironment. Autophagy is a mechanism involved in the regulation of this initial response and its manipulation can modify the progression of liver damage.

## Introduction

Chronic liver injury from any source leads to progressive fibrosis, yet treatments are elusive. A better understanding of the early changes following liver injury that disrupt cellular homeostasis, initiate and perpetuate fibrogenesis remains an unmet need. Liver sinusoidal endothelial cells (LSEC) constitute the liver's first defense barrier due to their unique position lining the sinusoidal lumen, and are the initial liver cell type to sense injury. Maintenance of the LSEC phenotype associated with cellular pores, or fenestrae, is critical to maintaining homeostasis in the whole liver parenchyma. Following hepatic damage, sinusoidal endothelial dysfunction (ED) may arise and it is characterized by the loss of both fenestrae (capillarization) and of its anti-fibrotic, antithrombotic and anti-vasodilatory properties, which are essential for the maintenance of liver integrity<sup>1</sup>. LSEC injury also plays an essential role in initiation and progression of liver injury. Indeed, signals derived from the sinusoidal endothelium during liver damage determine the outcome of pro-regenerative versus pro-fibrotic processes<sup>2,3</sup>. Despite its primary role in maladaptive healing and liver fibrosis<sup>4,5</sup>, the phenotypic regulation of ED is not fully understood.

Autophagy is a major intracellular recycling system that maintains cellular homeostasis under basal conditions, and plays an integral role in regulating the cellular adaptive response during stress<sup>6</sup>. Although autophagy has been implicated in the regulation of other resident liver cells (hepatocytes<sup>7</sup>, stellate cells<sup>8</sup> and macrophages<sup>9,10</sup>) and cardiovascular endothelial cell biology and physiopathology<sup>11</sup>, its role regulating liver endothelial phenotype during acute liver injury remains largely unknown.

In the present study we hypothesized that endothelial autophagy is an endogenous protective system whose loss could undermine LSEC integrity and phenotype, ultimately leading to liver fibrosis. Therefore, the aim of our study was to investigate the role of autophagy in the regulation of endothelial dysfunction and the impact of its manipulation during liver injury.

## Materials and methods:

### Animals

Animals were housed in polycarbonate cages and maintained in a temperature and light controlled facility under standard food and water *ad libitum*. All procedures were performed in accordance with Spanish legislation and approved by the Animal Research Committee of the University of Barcelona and were conducted in

accordance with the European Community guidelines for the protection of animals used for experimental and other scientific purposes (EEC Directive 86/609).

*Generation of endothelial Cell-specific Atg7 knockout mice:* Previously described Atg7<sup>Flox/Flox</sup> mice on the C57BL/6 background<sup>12</sup> were crossed with a line expressing Cre recombinase under the control of the VE-Cadherin promoter to generate Atg7-VE-Cadherin-Cre (Atg7<sup>endo</sup>) mice, a mouse model with a selective deficiency of the essential autophagy gene Atg7 in endothelial cells.

*Induction of fibrosis in mice:* Carbon tetrachloride (CCl<sub>4</sub>) (Sigma) was used to induce mild acute liver injury. Mice received 3 intraperitoneal (i.p.) injections of 10% CCl<sub>4</sub> (diluted in olive oil) at a dose of 0.5  $\mu$ L/g body weight<sup>13</sup> or vehicle (olive oil) every other day during one week<sup>8</sup>. Animals were sacrificed 48 hours after the last dose under ketamine/midazolam anesthesia. At least 5 animals per group were used in isolation experiments and 6 to 12 animals per group in total tissue experiments making a total of 81 mice analyzed. All experiments were performed with mice between 10-14 weeks of age. We analyzed the effect of liver injury in male and female mice and the effect was similar in both genders, so all subsequent experiments were performed indistinctly in male and female mice.

*Induction of fibrosis in rats:* Hepatic injury was induced in 250–300 g male Sprague-Dawley (SD) rats (Charles River) by CCl<sub>4</sub> (50% CCl<sub>4</sub> diluted in olive oil at a dose of 1  $\mu$ L/g of body weight) with three i.p. injections per week during 1, 4 or 6 weeks and compared with control rats injected with vehicle (olive oil)<sup>13</sup>. A minimum of 3 animals per group were used in isolation experiments accounting for a total of 36 rats. Animals were sacrificed 48 hours after the last dose (CCl<sub>4</sub>) under ketamine/midazolam anesthesia.

#### Cell lines and culture conditions

Unless otherwise specified, chemicals were purchased from Sigma-Aldrich (St. Louis, MO, USA). Culture media and supplements for cell culture were from Gibco-Invitrogen (Carlsbad, CA, USA) and plastic ware was from TPP (Trasadingen, Switzerland). Human Umbilical Vein Endothelial Cells (HUVEC, Lonza) were cultured on gelatin coating with M-199 (Gibco) medium supplemented with 20% FBS, 1% L-Glutamine, 1% PS and 1% ECGS. Mouse liver sinusoidal endothelial cells TSEC were kindly provided by Dr. V Shah<sup>14</sup> and cultured with endothelial cell medium (ECM, ScienCell) with 5% FBS, 1% PS and 1% ECGS. Rat and mouse LSEC as well as mouse hepatic stellate cells (HSC) were isolated as previously described<sup>15,16</sup>. In brief,

livers were perfused through the portal vein and digested with a collagenase solution. After mincing the liver, cells were filtered and centrifuged at 50 xg to remove hepatocytes. Non-parenchymal cells were then separated by differential centrifugation using a Percoll gradient. Kupffer cells were eliminated by plastic pre-culture during 30 min. LSEC were plated in collagen coating dishes in RPMI-1640 medium with 10% FBS, 1% L-Glutamine, 1% PS, 1% Fungizone (Reactiva) and 1% ECGS. HSC cells were cultured in DMEM/F12 with 20% FBS, 1% PS and 1% Fungizone.

*ROS induction studies:* HUVEC and TSEC were seeded in 6-well plates and grown for 24 h before treatment with hydrogen peroxide (0.25 and 120  $\mu$ M, respectively) and collected after 72 h.

#### Western blotting

Extracted proteins were analyzed by western-blot (wb). Antibodies used were: SQSTM1/p62 (Cell Signalling, 1/1000), LC3B (Cell Signalling, 1/1000), ATG7 (Cell signaling, 1/1000),  $\alpha$ -SMA (Sigma, 1/1000), PDGFR- $\beta$  (Santa Cruz, 1/500), total eNOS (BD Bioscience, 1/1000), eNOS phosphorylated Ser1177 (Cell Signalling, 1/1000), HO-1 (Enzo Life Sciences, 1/1000), NQO1 (Abcam, 1/1000). GAPDH (Santa Cruz, 1/1000) and  $\beta$ -actin (Sigma, 1/1000) served as housekeeping controls. Images were acquired with a LAS-3000 apparatus (Fujifilm, TDI, Alcobendas, Spain) and measurements made with the Multi Gauge software from Fujifilm following manufacturer's instructions. Protein ratios were normalized to housekeeping proteins ( $\beta$ -actin or GAPDH) and fold change was calculated relative to control group.

*Autophagy flux:* As autophagy is a dynamic process influenced by the degradation activity of the cargo and recycling, autophagic flux was measured using the lysosomal inhibitor Chloroquine (CQ) (20  $\mu$ M) 2 h. Briefly, CQ inhibits degradation of the cargo in the autophagosome leading to the accumulation of autophagic vacuoles (AV) that can be measured quantifying by WB the lipidated form of MAP1LC3/LC3 (microtubule-associated protein 1 light chain 3) (LC3II) present in the AV membrane.

#### Quantitative Real-Time Polymerase Chain Reaction

Total RNA was isolated by RNeasy Micro and Mini kit (Qiagen). First-strand cDNA was synthesized using the QuantiTect Reverse transcription kit (Qiagen) according to the manufacturer's instructions. Quantitative Real-Time Polymerase Chain Reaction (qRT-PCR) was performed using either Taqman Universal Master Mix or PowerUp SYBR Green Master Mix (Applied biosystems) with technical duplicates using an ABI Prism 7900 HT Cycler (Applied Biosystems). PCR cycle parameters were as follows: 95°C for 10' followed by 40 cycles at 95°C for 15" and 60°C for 1'. Results



were obtained with the Sequence Detection System 3.2 software (Applied Biosystems) and further analyzed by the  $2^{-\Delta\Delta C_t}$  method. GAPDH or  $\beta$ -ACTIN was used as a loading control. Results are shown as fold-change relative to the control group.

Primer specific sequences are listed in Suppl. Material.

#### Lentiviral Atg7 Small Interfering RNA Construction

Lentiviral supernatants of Small hairpin (sense-loop-antisense) RNAs against mouse Atg7 (siAtg7) and its corresponding empty vector (VEC) were a kind gift from Dr. Czaja<sup>8,17</sup>. TSEC cells were transduced with lentivirus for 24 h followed by puromycin selection. Cultures were more than 90% GFP positive at the time experiments were performed.

#### Histologic and Immunohistochemical studies

Liver samples were formalin fixed, paraffin embedded and 4  $\mu$ m sections obtained. Haematoxylin-eosin (H-E) staining was performed for structural analysis. Sirius Red was used to determine collagen deposition; sections were stained with Sirius Red solution (saturated picric acid containing 0.1% Direct Red 80) to visualize collagen. The red stained area per total area was determined using AxioVision software and values are expressed as the mean of 10 fields at 20x magnification obtained with a Zeiss Axiovert 135 microscope.

Immunohistochemical staining of  $\alpha$ SMA, Von Willebrand Factor (VWF) and desmin were performed with anti- $\alpha$ -SMA (1/200, Abcam), anti-VWF (1/100, Dako) and anti-desmin (1/100, Dako). Bound antibodies were visualized with Dako Real Envision Detection System Peroxidase/DAB+ kit, and slides were counterstained with haematoxylin. Fifteen images at 20x magnifications were captured for IHC quantification with a Zeiss Axiovert 135 microscope and quantified with Image J software.

#### Histological analysis

Histological analysis of the samples was performed on H-E stained slides by an expert pathologist. The inflammatory infiltrates in the liver parenchyma were evaluated in the portal, pericentral and lobular area using a score from 0-3 according to the following criteria: 0=none; 1=mild; 2=moderate; 3=severe. The regenerative aspect of hepatocytes was determined considering the peculiarity of these cells nucleus with the presence of diploid hepatocytes and an open chromatin, plus the number of mitosis in the liver parenchyma. The assessment of necrosis was performed as follows: 1= <5%;



2= 5-29%; 3=>30% of the analyzed parenchyma. Ballooning of hepatocytes was considered as 1 (mild) when it represented <4%, 2 (moderate) when it represented between 5 and 15% of the hepatic cells and finally, 3 (marked) when ballooning was seen in >15% of the liver parenchyma.

#### Hydroxyproline content

Hydroxyproline content was measured with Hydroxyproline Colorimetric Assay Kit (Biovision) following manufacturer's instructions.

Briefly, liver tissues were homogenized in H<sub>2</sub>O milli-Q. HCl (12 M) was added to the homogenate and samples were incubated at 120°C for 3 h. Kit reagents were added and absorbance at 560 nm was read in a plate reader and expressed as ng of hydroxyproline/mg liver.

#### Electron microscopy

Livers were perfused through portal vein with a fixation solution containing 2.5% glutaraldehyde and 2% paraformaldehyde in 0.1 M sodium cacodylate, pH 7.4 and fixed overnight at 4°C. Samples were washed three times with 0.1 M cacodylate buffer.

Transmission electron microscopy (TEM) was used to quantify the number of autophagosomes in LSEC. For TEM studies, fixed samples were then treated with 1% osmium tetroxide for 1 h, followed by dehydration in acetone gradients and embedded in Spurr resin. Ultrathin sections (50 nm) were counterstained with uranyl acetate and lead citrate<sup>18</sup>. Samples were analyzed using a JEOL J1010 electron microscope with an ORIUS camera (Gatan, Inc.; Roper Technologies, Inc.).

Scanning Electron Microscopy (SEM) was used to quantify liver sinusoidal fenestrae. Liver sections were fixed with 1% osmium in cacodylate buffer, dehydrated in ethanol, and dried with hexamethyldisilazane. Blocks were mounted onto stubs, and sputter coated with gold. Ten images per animal were acquired at a resolution of 15,000x using a Jeol 6380 Scanning Electron Microscope (JEOL Ltd, Tokyo, Japan). Liver sinusoidal fenestrations were quantified using Image J Software (NIH)<sup>18</sup>. Porosity (percentage of LSEC surface occupied by fenestrae) was measured in SEM in liver tissue; in brief, total surface area and the open area of individual fenestrae were quantified.

#### Measurement of the cellular superoxide content in liver tissue

*In situ* superoxide (O<sub>2</sub><sup>-</sup>) levels were assessed in HUVEC previously treated with either rapamycin or CQ, siAtg7 TSEC cells and in fresh liver cryosections (10 µm) obtained from Atg7<sup>endo</sup> and control mice, with the oxidative fluorescent dye

dihydroethidium (DHE; Molecular Probes Inc.) as described<sup>19</sup>. Six fields at 20x from each condition were randomly selected. Fluorescent images were obtained with an Inverted microscope Zeiss Axiovert and quantitative analysis was performed with Image J. In each experiment the same threshold was set for all images and integrated density (the product of Area and Mean Gray Value) was measured. For HUVEC and TSEC intensity was normalized to numbers of nuclei in each image.

#### Cyclic Guanosine Monophosphate (cGMP) Levels

Levels of GMPc were measured as a marker of nitric oxide bioavailability in liver homogenates using an enzyme immunoassay following manufacturer instructions (Cayman Chemical Co., Ann Arbor, MI)<sup>19</sup>. Briefly, equal amounts of liver tissue were dropped into 10 volumes of 5% trichloroacetic acid and homogenized at 4°C. The precipitate was removed by centrifugation at 2000g for 15 minutes at 4°C. The supernatant was transferred to a clean test tube, washed with water-saturated diethyl ether three times and lyophilized. The dried extract was dissolved in assay buffer and cGMP levels were determined by enzyme immunoassay. Results were expressed as picomoles/gram liver.

#### Nitrotyrosine fluorohistochemistry.

Quantitative tyrosine nitration detection was assessed as previously described<sup>20,21</sup>. Briefly, slides of liver sections were deparaffinized, hydrated, incubated with aqueous sodium dithionite solution (10 mM) for 10 min, washed with distilled water and then incubated overnight at 4°C with an equimolar solution of AlCl<sub>3</sub> and salicylaldehyde (200mM). Next morning, the aqueous solution was removed and sections were mounted in Fluoromount G medium (Southern Biotech, Birmingham, AL). Negative and positive internal controls were included. Fluorescence images were obtained with a fluorescence microscope OLYMPUS BX51 and quantitative analysis of at least six images per sample was performed with Image J.

#### Immunofluorescence

LSEC were seeded onto 12 mm micro coverglasses (Electron Microscopy Sciences). At different timepoints (0h, 24h, 48h) cells were fixed with 4% paraformaldehyde for 10 minutes at room temperature, rinsed with PBS and permeabilized with 0.1% triton X-100 (Sigma) for 5 minutes. Thereafter, cells were blocked for 30 minutes with 1% BSA in PBS and consequently incubated with primary antibodies against LC3B (1:200, cell signaling) and Lamp2 (1:100, Santa Cruz) overnight at 4°C.

Incubation with secondary antibodies conjugated with Alexa Fluor 488/555 (1:300, Invitrogen) was performed at room temperature for 1h along with DAPI (3ng/mL, Invitrogen). Preparations were then mounted using Fluoromount-G (Bionovacentifica) and dried overnight. Eight images per preparation and channel (visible; green, 488nm; red, 555nm) were obtained acquiring confocal z-stacks with a spectral confocal microscope (Leica TCS SPE). Images were then analyzed with the ImageJ software (NIH) calculating the Pearson's coefficient per cell. The Pearson's correlation coefficient is a quantitative measurement that estimates the degree of overlap between fluorescence signals obtained in the two channels (green and red). The Pearson coefficients were averaged, and a standard error of the mean was calculated<sup>22</sup>.

### Statistical analysis

Statistical analysis was performed using SPSS 23.0 or GraphPad 5.01 for Windows. Groups were compared by analysis of variance (ANOVA) with post-hoc tests when ANOVA analysis was significant (LSD and Tukey correction) or Student's t-test when comparing two groups as adequate. All data are reported as means  $\pm$  SEM. Differences were considered significant at a  $p$  value  $\leq 0.05$  with power of 80%.

### Results

#### *Autophagy is up-regulated during LSEC capillarization in vitro and in vivo*

After 24 h of growth on plastic in culture, isolated LSEC typically lose their fenestrated phenotype<sup>4</sup>; in the absence of growth factors, they become dysfunctional by 48 hours and lose viability<sup>23</sup>. To link these changes to autophagic activity, freshly isolated LSEC from untreated SD rats were cultured up to 48 hours on collagen-coated plastic. After 24 hours in culture, LSEC expressed the previously reported typical transcriptional changes that accompany capillarization *in vitro*<sup>4,24,25</sup>, which include the downregulated expression of *Vascular Endothelial Growth Factor Receptor 2* (VEGFR-2) and up-regulation of *endothelin-1* mRNAs (ET-1) (Fig 1A). These changes were accompanied by increased autophagic activity. As seen in Figure 1B, primary LSEC cultured for 24 hours demonstrated enhanced autophagic flux based on an increase of LC3II levels in the presence of the autophagy inhibitor chloroquine (CQ) (Fig 1B) and colocalization of LC3 and LAMP2 (Fig 1C). However, after longer periods of culture (48 hours) when LSEC are completely dysfunctional, autophagy levels began declining (Fig 1B, 1C).

Because *in vitro* experiments, even using freshly isolated LSEC, may not adequately represent the complexity of LSEC defenestration process, we determined

whether autophagic activity increases during ED *in vivo* after liver injury. SD rats were treated with CCl<sub>4</sub> (i.p. injection every other day) at different time-points and the grade of liver fibrosis was assessed. Whereas one-week of CCl<sub>4</sub> did not induce either ED or autophagy (data not shown), after 4 weeks mild fibrosis was induced and after 6 weeks fibrosis was severe; thus *in vivo* studies were conducted at 4 and 6 weeks. Cells isolated from SD rats with CCl<sub>4</sub>-induced mild fibrosis (4 weeks) or severe fibrosis (6 weeks) developed an abnormal phenotype characterized by down-regulation of VEGFR-2 and up-regulation of ET-1 mRNAs (Fig 1C). LSEC from rats with mild fibrosis displayed an augmented autophagy flux that recapitulated their *in vitro* response, but was unable to further increase when fibrosis was more severe (6 weeks) (Fig 1D), implicating a role of endothelial autophagy during early phases of liver injury. Also in agreement with this observation, when dysfunctional LSEC isolated from rats with CCl<sub>4</sub>-induced mild fibrosis were cultivated on plastic, they were unable to further up-regulate autophagy levels (Suppl. Fig 1).

These data suggest that up-regulation of endothelial autophagy may play a role in the adaptive response at early stages of liver injury, but it is overcome if the damage persists, and thus ED arises.

#### *Endothelial autophagy maintains LSEC homeostasis*

We next addressed the prospect that endothelial autophagy might regulate the phenotype of LSEC and orchestrate the early response to liver injury. To determine the role of endothelial autophagy during liver fibrosis *in vivo*, we generated a transgenic mouse line in which expression of the essential autophagy gene Atg7 was specifically deleted in endothelial cells (Atg7<sup>endo</sup> mice) (Fig 2). As previously described<sup>12</sup>, Atg7<sup>flox/flox</sup> mice<sup>26</sup> were crossed with mice carrying the Cre recombinase under the endothelial specific promoter VE-cadherin (Jackson laboratory) (Fig 2A). Primary LSEC were isolated from the Atg7<sup>endo</sup> mice and Atg7 knockdown was confirmed by immunoblotting and quantitative real-time polymerase chain reaction (Fig 2B,C). In agreement with previous studies<sup>26</sup>, LSEC isolated from Atg7<sup>endo</sup> mice displayed a down-regulation of autophagy levels, indicated by a reduced number of autophagic vacuoles (AVs) compared with their control littermates (Atg7<sup>control</sup>) when quantified by electron microscopy (Supl. Fig 3), accumulation of p62 and decrease LC3BII/I ratio measured by western blott (Fig 2D).

At baseline, mice with autophagy-defective LSEC (Atg7<sup>endo</sup>) displayed a normal liver architecture (Fig 3A) without hepatocyte injury (Fig 3B) and did not show an obvious phenotype beyond a reduced body weight (Fig 3C) when compared with their

control littermates (Atg7<sup>control</sup>). However, following mild acute liver injury (1 week of CCl<sub>4</sub>)<sup>8</sup> Atg7<sup>endo</sup> mice developed amplified ED (Fig 4) as evidenced by the up-regulation of mRNA levels of ET-1 and down-regulation of VEGFR-2 (Fig 4A). Although these mRNAs have been proposed as surrogate markers of capillarization, it remained critical to evaluate the actual loss of fenestrae by scanning electron microscopy (SEM)<sup>27,28</sup>, which is considered the gold standard technique for this purpose. SEM enables the assessment of large areas of the endothelial surface and measurement of size, frequency and porosity (the percentage of LSEC membrane that is occupied by fenestrations)<sup>4,18,28,29</sup>. SEM analysis confirmed a significant decrease in porosity and the number of fenestrae (Fig 4B), further confirming the greater level of endothelial dysfunction in the Atg7<sup>endo</sup> mice after mild acute liver injury. We also evaluated ED in whole liver tissue by quantifying levels of the glycoprotein von Willebrand Factor (vWF), which were increased, consistent with a more dysfunctional phenotype (Fig 4C).

Together, these data confirm that endothelial autophagy impairment provokes ED, suggesting that as in other cells, autophagy may be an adaptive response to stress.

#### *Loss of endothelial autophagy aggravates liver fibrosis without affecting liver inflammation*

We next evaluated the role of autophagy in fibrosis after mild acute liver injury. In Atg7<sup>endo</sup> mice liver fibrosis was greatly amplified when compared with Atg7<sup>control</sup> mice (Fig 5). Collagen accumulation evaluated by Sirius Red and hydroxyproline content was increased (Fig 5A), together with the increased expression of the HSC activation marker alpha-SMA, as evaluated both by western blot analysis of primary isolated HSC and total liver immunohistochemistry (Fig 5B). In contrast, there were no differences in the expression of desmin (Fig 5C) or the proliferation marker beta-PDGFR (Fig 5D), suggesting that the effect on fibrosis was due to activation of HSC and not an increase in the total HSC number or their proliferation. Interestingly, Atg7<sup>endo</sup> mice had conserved regenerative capacity (Fig 5E) and similar degree of liver injury than Atg7<sup>control</sup> (Fig 5E,F).

Interestingly, mild acute liver injury did not modify liver inflammation in our Atg7<sup>endo</sup> mice compared with Atg7<sup>control</sup> mice. Acute CCl<sub>4</sub>-induced injury induced mild pericentral inflammation similarly in the two groups of animals (Fig 5G,H).

These results suggest that endothelial autophagy impairment under stress conditions (mild acute liver injury) aggravates liver fibrosis by directly activating HSC.

*Loss of LSEC autophagy is associated with an insufficient antioxidant response*

Reduction in endothelial nitric oxide (NO) bioavailability has been identified as one of the main governors of LSEC defenestration. Both a decrease in NO production and an increase in the reactive oxygen species superoxide, which reacts rapidly with NO to form peroxynitrite, provoke reduction in NO bioavailability. Moreover, oxidative stress plays a central role in the development and progression of liver fibrosis<sup>19</sup> by inducing oxidative injury and endothelial dysfunction<sup>30,31</sup>. Because autophagy has been identified as a major mechanism, which protects cells from oxidative stress in a wide range of cells<sup>32–35</sup>, we reasoned that autophagy might help to maintain LSEC phenotype providing an adequate redox balance in endothelial cells.

To mimic the effect of intracellular oxidative stress generation, we directly stimulated endothelial cells with exogenous H<sub>2</sub>O<sub>2</sub>. We used two different cell lines, human endothelial cells (HUVEC) and mouse LSEC (TSEC). H<sub>2</sub>O<sub>2</sub> provoked an up-regulation in autophagy in both cell lines (Suppl Fig 2).

We therefore examined if pharmacological manipulation of endothelial autophagy modified oxidative stress. HUVEC were treated with the autophagy inhibitor CQ (Fig 6A) or the autophagy inducer rapamycin (Suppl. Fig 3) and O<sub>2</sub><sup>-</sup> levels were measured by DHE; this data show that inhibition of autophagy increases oxidative stress, which was attenuated when autophagy was up-regulated. To establish a more specific link between autophagy and oxidant injury, TSEC cells were transduced with a lentiviral vector expressing small hairpin RNA to Atg7 (siAtg7 cells) or with an empty lentivirus control (VEC) (Suppl. Fig 4). As predicted, genetic deletion of Atg7 amplified O<sub>2</sub><sup>-</sup> levels (Fig 6B), further suggesting that endothelial autophagy maintains liver homeostasis at least in part by alleviating oxidative stress.

We next corroborated these data *in vivo* by evaluating oxidative stress levels in Atg7<sup>endo</sup> mice after mild acute liver injury. Intracellular O<sub>2</sub><sup>-</sup> production measured by DHE (Fig 6C) and the content of hepatic nitrotyrosinate proteins, a fingerprint of peroxynitrite formation and a marker of NO scavenging by O<sub>2</sub><sup>-</sup> were markedly elevated (Fig 6D) in whole liver tissue of the Atg7<sup>endo</sup> mice compared to Atg7<sup>control</sup> mice suggesting a decreased NO bioavailability. Indeed, cyclin guanosine monophosphate (c-GMP) a marker of intrahepatic NO availability, was significantly reduced in the Atg7<sup>endo</sup> mice compared to Atg7<sup>control</sup> mice (Fig 6E).

Reduction in NO bioavailability may result from a decrease in endothelial NO production but also from impaired ROS removal<sup>14–18</sup>. Furthermore, recent data in vascular endothelial cells from kidney and the cardiovascular system have demonstrated that autophagy regulates eNOS production<sup>19–22</sup>. We therefore examined whether inhibition of autophagy impairs NO production in our endothelial autophagy-



deficient mice after CCl<sub>4</sub> induced liver injury. Decreased NO production due to reduced eNOS activity (measured by eNOS phosphorylationSer1177/eNOS total ratio) was observed in the Atg7<sup>endo</sup> mice compared to Atg7<sup>control</sup> mice (Fig.6F) suggesting that endothelial autophagy helps to cope with CCl<sub>4</sub>-induced oxidative stress by directly regulating intrahepatic NO bioavailability.

However, autophagy may control the antioxidant response in LSEC by additionally removing oxidative species. We evaluated the detoxifying response of LSECs after mild acute liver injury. We evaluated the classical antioxidant enzymes, superoxide dismutase (SOD), catalase (CAT) and glutathione peroxidase (GPx), in primary isolated LSEC from Atg7<sup>endo</sup> and Atg7<sup>control</sup> mice after acute CCl<sub>4</sub>-induced injury. As shown in figure 7A, a significant downregulation in these protective genes was observed. The antioxidant activity of these genes in whole liver tissue was also insufficient to alleviate the accumulation of oxidative species provoked by endothelial-specific autophagy impairment, reinforcing the importance of LSEC as the main scavenger cell type of the liver (Suppl. Fig 5).

The activity of the classical antioxidant genes can be bolstered by the so-called 'phase II detoxifying enzymes' regulated by the nuclear factor-erythroid 2-related factor 2 (Nrf2). Under oxidative stress, Nrf2 is phosphorylated and translocates into the nucleus, where it interacts with the antioxidant response element (ARE) within the promoters of genes encoding NADPH: quinone oxidoreductase 1 (Nqo1), heme oxygenase-1 (HO-1) glutathione S transferase mu subunit (Gstm), glutamate- cysteine ligase catalytic (Gclc) and modulatory (Gclm) subunits and sulfiredoxin-1 (Srxn1)<sup>36,37</sup>. Besides, Nrf2 can also be activated by the cytosolic protein p62 in conditions of autophagy deficiency. P62 degradation is impaired when autophagy is compromised and dissociates the redox-sensitive transcription complex Nrf2-Keap1, allowing Nrf2 translocation to the nucleus and activation of the ARE genes transcription<sup>38,39</sup>. Indeed, as shown in Figure 7B, the Nrf2-mediated antioxidant response in autophagy-deficient LSEC was upregulated, but was not sufficient to counteract the elevated oxidative stress, probably due at least in part by the shortage in NO. We also evaluated two of the main Nrf2-targets and further verify its upregulation at protein level (Fig.7C), as an attempt to remove ROS in the Atg7<sup>endo</sup> mice. Remarkably, the Nrf2-mediated antioxidant response was unchanged in whole liver tissue, emphasizing the concept that impaired autophagy is the main trigger for Nrf2 activation and its activation may be limited to autophagy-deficient cells (Suppl. Fig 5).

All together these data support the concept that autophagy regulates LSEC response to oxidative stress by regulating both NO bioavailability and ROS removal.



## Discussion

Capillarization of sinusoids represents a change in LSEC phenotype characterized by the loss of fenestration, which induces HSC activation and liver fibrogenesis<sup>1</sup>. Although HSC can be activated through other mechanisms during liver injury, signals coming from the endothelium determine and orchestrate the early liver response to a given injury<sup>2,3</sup>. Preventing ED is an attractive therapeutic strategy that could interrupt progression to liver fibrosis; however, the mechanisms controlling LSEC phenotypic changes are still not fully understood.

Our findings demonstrate that autophagic activity modulates LSEC capillarization. Loss of autophagy selectively in LSEC amplifies ED and activates HSC following mild acute liver injury. Basal autophagy in LSEC, as in other cells of the liver<sup>40</sup> is low, but it is rapidly upregulated as an adaptive response under conditions of cellular stress both *in vitro* and *in vivo*. In our Atg7<sup>endo</sup> mice, the moderate reduction of autophagy achieved in LSEC, may be sufficient to maintain adequate levels of endothelial autophagy under basal conditions to preserve a normal architecture. However, during early phases of the injury autophagy upregulation plays an important role maintaining LSEC phenotype. Indeed, if the insult is either too intense or persist over time, autophagy induction is overcome leading to ED and progressive fibrosis. In agreement with this concept, autophagy is rapidly upregulated in the hepatocytes following alcohol injury in alcoholic liver disease, but over time there is a gradual loss of autophagy function<sup>41</sup>, supporting the idea that autophagy plays an essential role in early phases of the pathological process.

Remarkably, loss of LSEC autophagy provokes not only an exacerbation of ED under conditions of cellular stress but also impacts the surrounding microenvironment by specifically modulating HSC activation. Indeed our transgenic animals did not have increased inflammation or prominent liver injury, supporting the concept that LSEC act as gatekeeper of HSC activation<sup>28,42</sup>.

NO has been previously identified as a master regulator of LSEC phenotype and contributes to maintaining redox balance. Because oxidant stress frequently accompanies liver injury and fibrogenesis and can induce autophagy<sup>43</sup>, we hypothesized that autophagy may preserve the LSEC phenotype at least in part by regulating NO, neutralizing ROS and maintaining cellular homeostasis. Indeed, exogenous ROS generation in endothelial cells was able to trigger autophagy. Moreover, disruption of endothelial autophagy, either pharmacologically or genetically, led to an aberrant antioxidant response and accumulation of ROS.

Our data also demonstrate that endothelial autophagy deficiency reduces intrahepatic NO bioavailability due to both decreased in production and increased scavenging, which impairs the antioxidant response. In conditions of liver injury and increased demands to maintain redox homeostasis, autophagy-deficient LSEC are incapable of increasing NO levels to maintain their phenotype, ROS accumulates and ED arises. LSEC are equipped with powerful antioxidant systems to remove ROS. The classical major regulators of cellular redox balance antioxidant enzyme (CAT, SOD and GPx) could not be upregulated in LSEC from our Atg7<sup>endo</sup> mice during mild acute liver injury leading to an inefficient adaptation to oxidative stress. This inability to cope with ROS, but autophagy loss triggers Nrf2 activation and ARE upregulation to foster a more intense antioxidant response. The increase in p62 levels that accompanies autophagy impairment dissociates the redox-sensitive transcription complex Nrf2-Keap1 and leads to increased stabilization, translocation to the nucleus and activation of the transcription of the antioxidant genes Nqo1, HO-1, Gstm, Gclc, Gclm and Srxn1<sup>39</sup>. The upregulation of these genes in the Atg7<sup>endo</sup> mice reinforces the idea that autophagy regulates the antioxidant response in LSEC. Altogether, our data support the idea that autophagy-deficient LSEC are unable to neutralize the antioxidant stress that accompanies liver injury, in part due to an inefficient antioxidant response and unavailability of maintaining adequate NO production. However, it remains to be elucidated whether upregulation of Nrf2 depends mainly on oxidant stress, autophagy deficiency or both.

Despite all the evidence supporting the association of oxidative stress and liver disease, how “antioxidant” compounds may regulate LSEC phenotype remains largely uncovered. Moreover, failure of antioxidant therapies in slowing fibrosis progression<sup>44–46</sup> in real clinical practice, favors the idea that interventions only removing ROS may not be enough. Indeed, we have shown that following acute CCl<sub>4</sub>-induced damage, LSEC de-differentiation due to autophagy dysfunction promoted decreased NO bioavailability, ROS accumulation and liver fibrogenesis, through HSC activation. Our data suggest that the inability of autophagy-deficient-LSEC to handle oxidative stress is responsible, at least in part, of promoting HSC activation; however, whether autophagy-mediated sinusoidal capillarization actively fosters HSC activation via release of specific paracrine mediators remains to be determined. Indeed, capillarized LSEC may contribute to HSC phenotypic and functional modulation not only by regulating NO production, but also secreting other pro-fibrotic factors<sup>2,3</sup>.

Notwithstanding these functions, autophagy may also alleviate oxidative stress by other additional mechanism such as removal of ROS-damaged organelles like mitochondria, endoplasmic reticulum... as it has been demonstrated in other cell types

but it deserves detailed future specific studies in LSEC. Moreover, autophagy may also regulate other cellular pathways in LSEC besides NO and the antioxidant response. Indeed a previous study from our group demonstrated that autophagy upregulates the transcription factor KLF2 during ischemia-reperfusion injury and modulates endothelial survival<sup>22</sup>. Recently, autophagy has also been implicated in LSEC defenestration by controlling caveolin-1 expression<sup>47</sup>.

In conclusion, our data demonstrate that autophagy contributes to maintain cellular phenotype and protects LSEC from oxidative stress during early phases of the liver injury, but may not be enough to revert damage in advanced stages of chronic liver injury. Endothelial autophagy dysregulation activates HSC and aggravates fibrosis during mild acute liver injury. Potentiation of autophagy selectively in LSEC during early stages of liver disease may be an attractive approach in order to prevent disease progression, thus modifying the natural course of chronic liver diseases.

## Figure Legends

**Figure 1. Autophagy is upregulated during *in vitro* and *in vivo* induced capillarization:** Primary LSEC were isolated from untreated SD rats, directly plated (t=0h) and grown on plastic tissue culture or onto coverglasses for 24 (t=24) and 48 h (t=48). Cells were then fixed and processed for immunofluorescent microscopy. For autophagy flux assay by wb cells were treated with CQ or vehicle during 2h and collected thereafter. (A) mRNA changes (qRT-PCR analysis) associated with endothelial dysfunction, showing a decrease in VEGFR2 and an increase in ET-1 and (B) LC3B II immunoblotting with and without addition of CQ showing an increase in autophagy flux at 24 h that decreases at 48 h of culture. (C) Representative immunofluorescent images and quantification of autophagosomes (LC3, green) with lysosomes (Lamp2, red) colocalization (R value) in LSEC confirming autophagy upregulation during capillarization. Primary LSEC isolated from rats treated with CCl<sub>4</sub> or vehicle for 4 and 6 weeks: (D) mRNA changes (qRT-PCR analysis) associated with endothelial dysfunction, showing a decrease in VEGFR2 and an increase in ET-1 and (E) LC3B II immunoblotting with and without addition of CQ showing autophagy flux displaying an increase at 4 weeks and incapability of further increase at 6 weeks. Data shows mean value  $\pm$  SEM of at least 3 experiments. mRNA and protein expressions are expressed as fold change relative to control (\*P $\leq$ 0.05, \*\*P $\leq$ 0.01, \*\*\*P $\leq$ 0.001, Student's t-test or analysis of variance (ANOVA)).

**Figure 2: Generation of Atg7<sup>endo</sup> mice.** (A) Schematic view of Atg7<sup>endo</sup> mice model generation. (B) mRNA changes (qRT-PCR analysis) and (C) immunoblot of primary LSEC isolated from Atg7<sup>endo</sup> mice showing decreased expression of Atg7 and LC3BII/I and increased of p62 levels. Data shows mean value  $\pm$  SEM of at least 3 experiments (\*P $\leq$ 0.05, \*\*P $\leq$ 0.01, \*\*\*P $\leq$ 0.001, Student's t-test).

**Figure 3. Loss of LSEC autophagy does not affect liver homeostasis.** (A) Representative images of whole liver H-E staining showing a normal liver architecture. (B) transaminase levels (n=12) and (C) animal body weight (n=69) from Atg7<sup>endo</sup> and Atg7<sup>contro</sup> mice under basal conditions. Data shows mean value  $\pm$  SEM. Protein expressions are expressed as fold change relative to control (\*P $\leq$ 0.05, \*\*P $\leq$ 0.01, \*\*\*P $\leq$ 0.001, Student's t-test).

**Figure 4. Loss of LSEC autophagy leads to cellular dysfunction.** Atg7<sup>endo</sup> and Atg7<sup>contro</sup> mice were treated every other day with CCl<sub>4</sub> i.p. for 1 week to induce mild acute liver injury. (A) mRNA changes (qRT-PCR analysis) associated with endothelial

dysfunction in primary isolated LSEC, showing a decrease in VEGFR2 and an increase in ET-1. (B) SEM representative graphs of LSEC from Atg7<sup>endo</sup> and Atg7<sup>control</sup> mice with porosity and number of fenestrae quantification, showing a loss of fenestrae (capillarization) in the Atg7<sup>endo</sup> mice. (C) Whole liver sections stained for the ED marker von Willebrand factor (vWF), displaying an increase value in Atg7<sup>endo</sup> mice. Data shows mean value  $\pm$  SEM (\*P $\leq$ 0.05, \*\*P $\leq$ 0.01, \*\*\*P $\leq$ 0.001, Student's t-test).

**Figure 5. Loss of LSEC autophagy amplifies liver fibrosis without increasing liver injury.** Atg7<sup>endo</sup> and Atg7<sup>control</sup> mice were treated every other day with CCl<sub>4</sub> i.p. for 1 week to induce mild acute liver injury (n=24). (A) Whole liver sections stained for Sirius Red and quantification of Sirius Red-positive area (left) and Hydroxyproline stain content (right). (B) Immunoblots for alpha-SMA in isolated HSC from Atg7<sup>endo</sup> and Atg7<sup>control</sup> mice and protein quantification (left) and whole liver sections stained for alpha-SMA and quantification of alpha-SMA positive area (right). (C) Whole liver sections stained for desmin and quantification of desmin-positive area. (D) Immunoblots for beta-PDGFR in whole liver from Atg7<sup>endo</sup> and Atg7<sup>control</sup> mice and protein quantification. (E) Transaminases levels showing an increase in AST without changing in ALT. (F) histological liver analysis for hepatocyte regenerative capacity and liver injury. (G) Histological liver analysis for inflammation scoring and (H) representative images of whole liver sections stained for H-E in Atg7<sup>endo</sup> and Atg7<sup>control</sup> mice after mild acute liver injury (CCl<sub>4</sub> i.p. for 1 week). Representative images are shown. Data shows mean value  $\pm$  SEM of at least 3 experiments (\*P $\leq$ 0.05, \*\*P $\leq$ 0.01, \*\*\*P $\leq$ 0.001, Student's t-test).

**Figure 6. Loss of LSEC autophagy increases oxidative stress and decreases NO bioavailability.** Cellular superoxide content measured by dihydroethidium (DHE) in (A) HUVEC pre-treated with Chloroquine during 12 h and H<sub>2</sub>O<sub>2</sub> was added during 15 h, (B) TSEC transduce with empty vector or siAtg7 were also treated with H<sub>2</sub>O<sub>2</sub> during 15 h and (C) in whole liver from Atg7<sup>endo</sup> and Atg7<sup>control</sup> mice after mild acute liver injury (CCl<sub>4</sub> i.p. for 1 week). (D) Quantitative nitrotyrosinated proteins analysis by fluorohistochemistry in whole liver tissue from Atg7<sup>endo</sup> and Atg7<sup>control</sup> mice after mild acute liver injury (CCl<sub>4</sub> i.p. for 1 week). (E) Cyclic guanosine monophosphate (cGMP) levels in liver homogenates from Atg7<sup>endo</sup> and Atg7<sup>control</sup> mice (CCl<sub>4</sub> i.p. for 1 week) illustrating a significant decrease. (F) Immunoblots for total eNOS and phosphorylated eNOS in whole liver from Atg7<sup>endo</sup> and Atg7<sup>control</sup> mice and protein quantification. Representative images are shown. Protein is expressed as fold change relative to

control. Data shows mean value  $\pm$  SEM of at least 3 experiments (\* $P \leq 0.05$ , \*\* $P \leq 0.01$ , \*\*\* $P \leq 0.001$ , Student's t-test).

**Figure 7. Loss of LSEC autophagy is associated with an insufficient antioxidant response.** Atg7<sup>endo</sup> and Atg7<sup>control</sup> mice were treated every other day with CCl<sub>4</sub> i.p. for 1 week to induce mild acute liver injury and primary LSEC were isolated. (A) mRNA changes (qRT-PCR analysis) showing a downregulation of the classical genes that protect against oxidative stress Gpx1, Gpx4, Sod1, Sod2 and catalase and (B) mRNA changes (qRT-PCR analysis) showing upregulation of the Nrf2-dependent antioxidative stress genes Srxn, Nqo1, Gclc, Gclm, and Gstm2. (C) Immunoblots for NQO1 and HO-1 in isolated LSEC from Atg7<sup>endo</sup> and Atg7<sup>control</sup> mice confirming an increase at the protein levels. Data shows mean value  $\pm$  SEM of at least 3 experiments. mRNA expression is expressed as fold change relative to control (\* $P \leq 0.05$ , \*\* $P \leq 0.01$ , \*\*\* $P \leq 0.001$ , Student's t-test).

#### List of Abbreviations.

Liver sinusoidal endothelial cells (LSEC)  
 Endothelial dysfunction (ED)  
 Carbon tetrachloride (CCl<sub>4</sub>)  
 Human Umbilical Vein Endothelial Cells (HUVEC)  
 Hepatic Stellate Cells (HSC)  
 Sprague-Dawley (SD)  
 Chloroquine (CQ)  
 Autophagic vacuoles (AV)  
 MAP1LC3/LC3 (microtubule-associated protein 1 light chain 3) (LC3II)  
 Transmission electron microscopy (TEM)  
 Scanning Electron Microscopy (SEM)  
 Superoxide (O<sub>2</sub><sup>-</sup>)  
 Dihydroethidium (DHE)  
 Analysis of variance (ANOVA)  
 Vascular Endothelial Growth Factor Receptor 2 (VEGFR-2)  
 Endothelin-1 (ET-1)  
 Conditioned medium (CM)  
 DMEM (Dulbecco's Modified Eagle Medium)  
 Intraperitoneal (i.p.)

#### Acknowledgments

The authors thank Biobank core facility of the Institut d'Investigacions Biomèdiques August Pi i Sunyer (IDIBAPS) for the technical help. We also thank Dr. Z Yue for the Atg7F/F mice, Dr. M. Czaja for the shAtg7 lentivirus and Dr. V Shah for the TSEC, Dr. A Diaz for the pathological support, J. Gracia-Sancho for experimental support, H Garcia-Caldero and M Monclús for their excellent technical assistance and R. Maeso for her experimental expertise. We also thank CERCA Programme / Generalitat de Catalunya.

## References

1. DeLeve, L. D., Wang, X. & Guo, Y. Sinusoidal endothelial cells prevent rat stellate cell activation and promote reversion to quiescence. *Hepatology* **48**, 920–930 (2008).
2. Ding, B.-S. *et al.* Divergent angiocrine signals from vascular niche balance liver regeneration and fibrosis. *Nature* **505**, 97–102 (2014).
3. Ding, B.-S. *et al.* Inductive angiocrine signals from sinusoidal endothelium are required for liver regeneration. *Nature* **468**, 310–315 (2010).
4. Xie, G. *et al.* Hedgehog signalling regulates liver sinusoidal endothelial cell capillarisation. *Gut* **62**, 299–309 (2013).
5. Pasarín, M. *et al.* Sinusoidal endothelial dysfunction precedes inflammation and fibrosis in a model of NAFLD. *PLoS One* **7**, e32785 (2012).
6. Kroemer, G., Mariño, G. & Levine, B. Autophagy and the Integrated Stress Response. *Mol. Cell* **40**, 280–293 (2010).
7. Singh, R. *et al.* Autophagy regulates lipid metabolism. *Nature* **458**, 1131–1135 (2009).
8. Hernández-Gea, V. *et al.* Autophagy Releases Lipid That Promotes Fibrogenesis by Activated Hepatic Stellate Cells in Mice and in Human Tissues. *Gastroenterology* **142**, 938–946 (2012).
9. Lodder, J. *et al.* Macrophage autophagy protects against liver fibrosis in mice. *Autophagy* **11**, 1280–1292 (2015).
10. Ilyas, G. *et al.* Macrophage autophagy limits acute toxic liver injury in mice through down regulation of interleukin-1 $\beta$ . *J. Hepatol.* **64**, 118–27 (2016).
11. Lavandero, S., Chiong, M., Rothermel, B. A. & Hill, J. A. Autophagy in cardiovascular biology. *J. Clin. Invest.* **125**, 55–64 (2015).
12. Torisu, T. *et al.* Autophagy regulates endothelial cell processing, maturation and secretion of von Willebrand factor. *Nat. Med.* **19**, 1281–7 (2013).



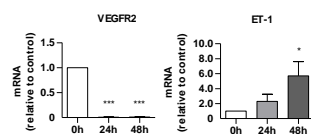
13. Ghiassi-Nejad, Z. *et al.* Reduced hepatic stellate cell expression of kruppel-like factor 6 tumor suppressor isoforms amplifies fibrosis during acute and chronic rodent liver injury. *Hepatology* **57**, 786–796 (2013).
14. Huebert, R. C. *et al.* Immortalized liver endothelial cells: a cell culture model for studies of motility and angiogenesis. *Lab. Investig.* **90**, 1770–1781 (2010).
15. Gracia-Sancho, J. *et al.* Enhanced vasoconstrictor prostanoid production by sinusoidal endothelial cells increases portal perfusion pressure in cirrhotic rat livers. *J. Hepatol.* **47**, 220–7 (2007).
16. Blomhoff, R. & Berg, T. Isolation and cultivation of rat liver stellate cells. *Methods Enzymol.* **190**, 58–71 (1990).
17. Singh, R. *et al.* Autophagy regulates adipose mass and differentiation in mice. *J. Clin. Invest.* **119**, 3329–39 (2009).
18. Le Couteur, D. G. *et al.* Pseudocapillarization and associated energy limitation in the aged rat liver. *Hepatology* **33**, 537–43 (2001).
19. Gracia-Sancho, J. *et al.* Increased oxidative stress in cirrhotic rat livers: A potential mechanism contributing to reduced nitric oxide bioavailability. *Hepatology* **47**, 1248–56 (2008).
20. Wisastra, R. *et al.* Antibody-free detection of protein tyrosine nitration in tissue sections. *Chembiochem* **12**, 2016–20 (2011).
21. Hide, D. *et al.* A novel form of the human manganese superoxide dismutase protects rat and human livers undergoing ischaemia and reperfusion injury. *Clin. Sci.* **127**, 527–537 (2014).
22. Guixé-Muntet, S. *et al.* Cross-talk between autophagy and KLF2 determines endothelial cell phenotype and microvascular function in acute liver injury. *J. Hepatol.* **66**, 86–94 (2017).
23. DeLeve, L. D., Wang, X., Hu, L., McCuskey, M. K. & McCuskey, R. S. Rat liver sinusoidal endothelial cell phenotype is maintained by paracrine and autocrine regulation. *Am. J. Physiol. Gastrointest. Liver Physiol.* **287**, G757-63 (2004).
24. Rockey, D. C. & Chung, J. J. Reduced nitric oxide production by endothelial cells in cirrhotic rat liver: endothelial dysfunction in portal hypertension. *Gastroenterology* **114**, 344–51 (1998).
25. Géraud, C. *et al.* Liver sinusoidal endothelium: A microenvironment-dependent differentiation program in rat including the novel junctional protein liver endothelial differentiation-associated protein-1. *Hepatology* **52**, 313–326 (2010).
26. Komatsu, M. *et al.* Impairment of starvation-induced and constitutive autophagy in Atg7-deficient mice. *J. Cell Biol.* **169**, 425–34 (2005).
27. Poisson, J. *et al.* Liver sinusoidal endothelial cells: Physiology and role in liver

- diseases. *J. Hepatol.* **66**, 212–227 (2017).
28. DeLeve, L. D. Liver sinusoidal endothelial cells in hepatic fibrosis. *Hepatology* **61**, 1740–1746 (2015).
29. Cogger, V. C., O'Reilly, J. N., Warren, A. & Le Couteur, D. G. A Standardized Method for the Analysis of Liver Sinusoidal Endothelial Cells and Their Fenestrations by Scanning Electron Microscopy. *J. Vis. Exp.* e52698 (2015). doi:10.3791/52698
30. Guillaume, M. *et al.* Recombinant human manganese superoxide dismutase reduces liver fibrosis and portal pressure in CCl<sub>4</sub>-cirrhotic rats. *J. Hepatol.* **58**, 240–246 (2013).
31. Di Pascoli, M. *et al.* Resveratrol improves intrahepatic endothelial dysfunction and reduces hepatic fibrosis and portal pressure in cirrhotic rats. *J. Hepatol.* **58**, 904–910 (2013).
32. Scherz-Shouval, R. *et al.* Reactive oxygen species are essential for autophagy and specifically regulate the activity of Atg4. *EMBO J.* **26**, 1749–60 (2007).
33. Mizushima, N. Autophagy: process and function. *Genes Dev.* **21**, 2861–2873 (2007).
34. Kroemer, G., Mariño, G. & Levine, B. Autophagy and the Integrated Stress Response. *Mol. Cell* **40**, 280–293 (2010).
35. Filomeni, G., De Zio, D. & Cecconi, F. Oxidative stress and autophagy: the clash between damage and metabolic needs. *Cell Death Differ.* **22**, 377–88 (2015).
36. Hernández-Gea, V. *et al.* Endoplasmic reticulum stress induces fibrogenic activity in hepatic stellate cells through autophagy. *J. Hepatol.* **59**, 98–104 (2013).
37. Marrone, G. *et al.* KLF2 exerts antifibrotic and vasoprotective effects in cirrhotic rat livers: behind the molecular mechanisms of statins. *Gut* **64**, 1434–43 (2015).
38. Puissant, A., Fenouille, N. & Auberger, P. When autophagy meets cancer through p62/SQSTM1. *Am. J. Cancer Res.* **2**, 397–413 (2012).
39. Komatsu, M. *et al.* The selective autophagy substrate p62 activates the stress responsive transcription factor Nrf2 through inactivation of Keap1. *Nat. Cell Biol.* **12**, 213–23 (2010).
40. Cuervo, A. M., Knecht, E., Terlecky, S. R. & Dice, J. F. Activation of a selective pathway of lysosomal proteolysis in rat liver by prolonged starvation. *Am. J. Physiol.* **269**, C1200-8 (1995).
41. Ding, W.-X., Li, M. & Yin, X.-M. Selective taste of ethanol-induced autophagy for mitochondria and lipid droplets. *Autophagy* **7**, 248–9 (2011).
42. Xie, G. *et al.* Role of differentiation of liver sinusoidal endothelial cells in

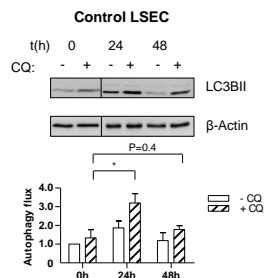
- progression and regression of hepatic fibrosis in rats. *Gastroenterology* **142**, 918–927.e6 (2012).
43. Chen, Y., Azad, M. B. & Gibson, S. B. Superoxide is the major reactive oxygen species regulating autophagy. *Cell Death Differ.* **16**, 1040–52 (2009).
  44. Sanyal, A. J. *et al.* Pioglitazone, Vitamin E, or Placebo for Nonalcoholic Steatohepatitis. *N. Engl. J. Med.* **362**, 1675–1685 (2010).
  45. Harrison, S. A., Torgerson, S., Hayashi, P., Ward, J. & Schenker, S. Vitamin E and vitamin C treatment improves fibrosis in patients with nonalcoholic steatohepatitis. *Am. J. Gastroenterol.* **98**, 2485–2490 (2003).
  46. Ferenci, P. *et al.* Randomized controlled trial of silymarin treatment in patients with cirrhosis of the liver. *J. Hepatol.* **9**, 105–13 (1989).
  47. Luo, X. *et al.* Autophagic degradation of caveolin-1 promotes liver sinusoidal endothelial cells defenestration. *Cell Death Dis.* **9**, 576 (2018).

# Autophagy is upregulated during *in vitro* and *in vivo* induced capillarization

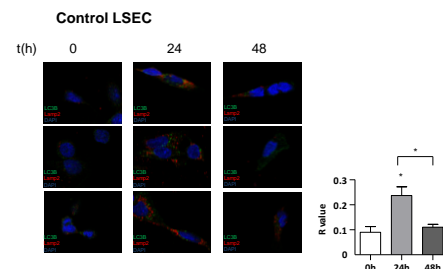
A



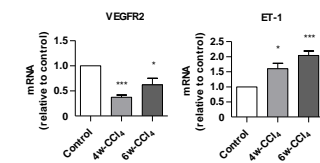
B



C



D



E

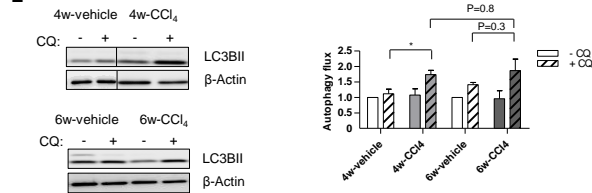
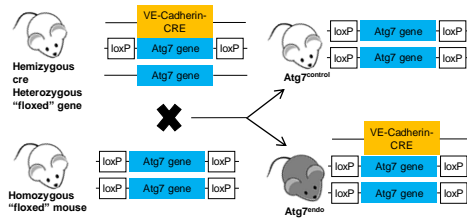


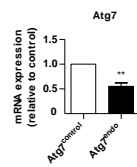
Figure 1

# Generation of Atg7<sup>endo</sup> mice

A



B



C

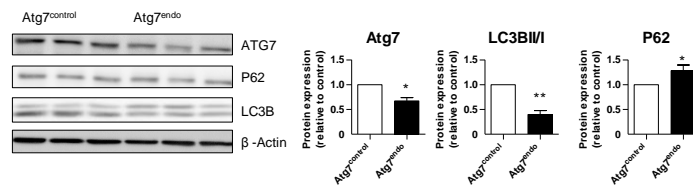
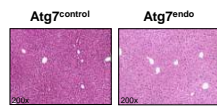


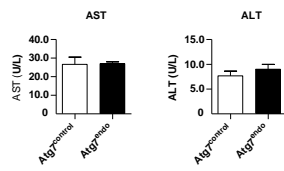
Figure 2

# Loss of LSEC autophagy does not affect normal liver homeostasis

A



B



C

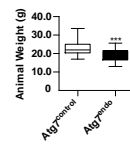


Figure 3

# Loss of LSEC autophagy leads to cellular dysfunction

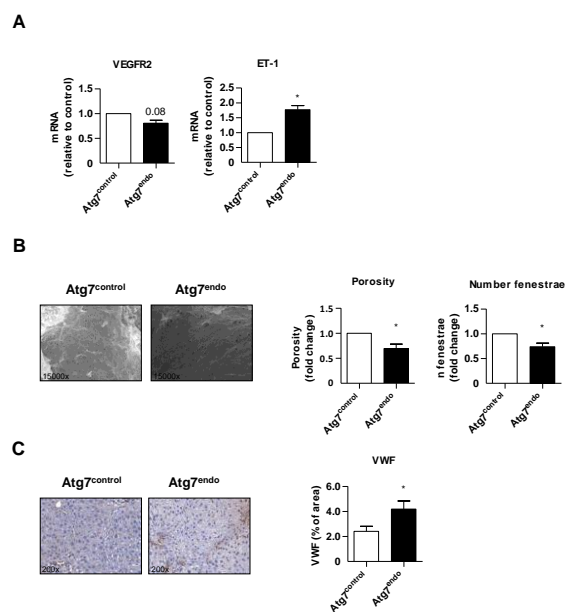


Figure 4



# Loss of endothelial autophagy amplifies liver fibrosis without increasing liver injury

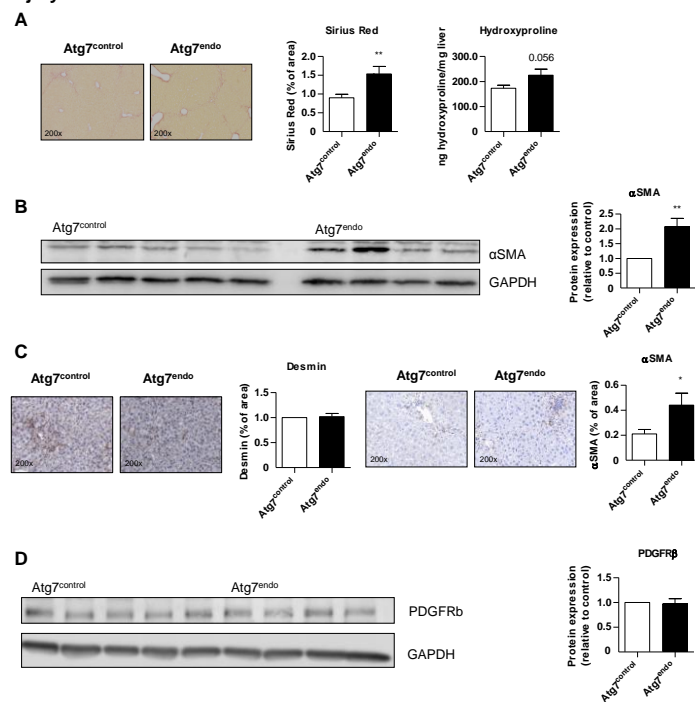
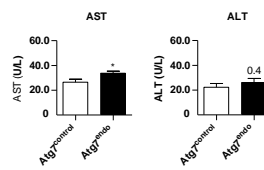


Figure 5

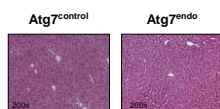
E

	Atg7 <sup>control</sup> (N=12)	Atg7 <sup>endo</sup> (N=12)
Regenerative Hepatocytes, n		
Yes/No	12/0	12/0
Necrosis, n		
0	5	6
1	0	2
2/3	7	4
Ballooning, n		
0	9	12
1	1	0
2/3	2	0

F



G



H

	Atg7 <sup>control</sup> (N=12)	Atg7 <sup>endo</sup> (N=12)
Lobular inflammation grade, n		
0	12	11
1	0	1
2/3	0	0
Periportal inflammation grade, n		
0	12	12
1	0	0
2/3	0	0
Pericentral inflammation grade, n		
0	3	4
1	9	8
2/3	0	0

Figure 5

# Loss of LSEC autophagy increases oxidative stress and decreases NO bioavailability

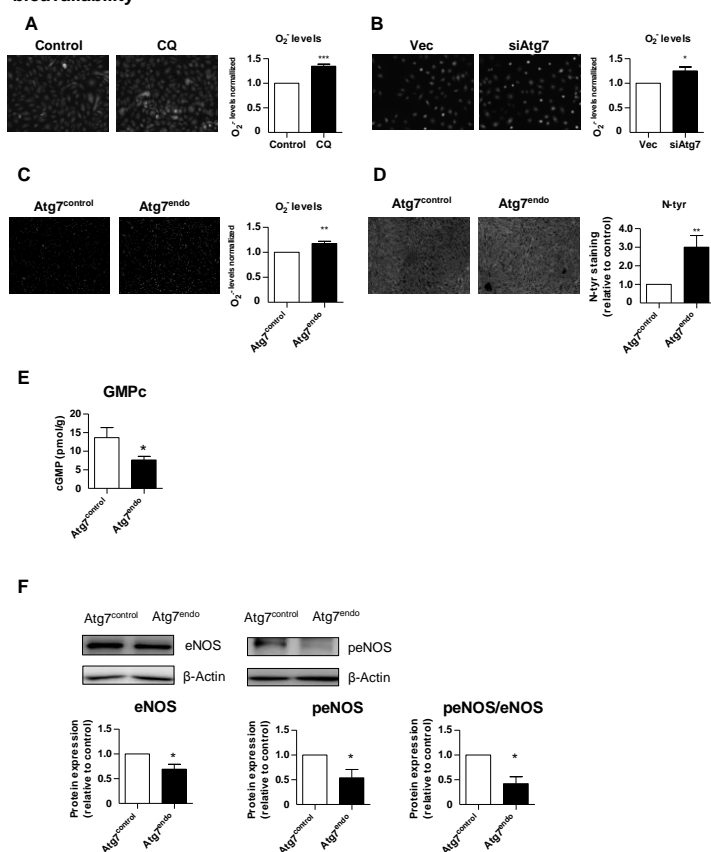


Figure 6

# Loss of LSEC autophagy is associated with an insufficient antioxidant response

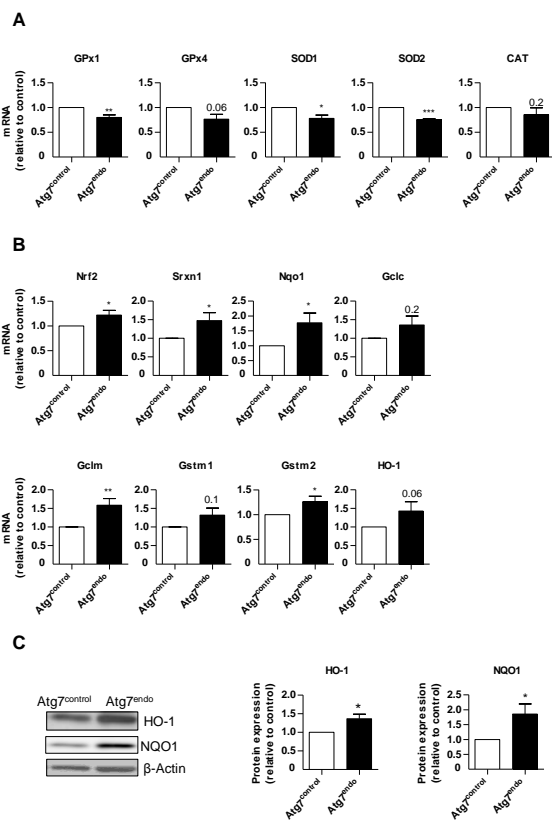


Figure 7

- Autophagy maintains liver endothelial cells homeostasis
- Autophagy deficiency in LSEC increases oxidative stress
- Autophagy regulates oxide nitric bioavailability and maintains LSEC phenotype
- Impairment of endothelial autophagy enhances endothelial dysfunction and exacerbates fibrosis

ACCEPTED MANUSCRIPT

